


Preclinical Evaluation of a Protein-Based Nanoscale Contrast Agent for MR Angiography at an Ultralow Dose

Jianmin Li^{1,2,*}, Wenyi Zhang^{1,2,*}, Shuang Liu^{1,2,*}, Fan Yang², Yupeng Zhou², Lin Cao^{1,2}, Yiming Li^{1,2}, Yunfei Guo^{1,2}, Xiang Qi^{1,2}, Guoping Xu¹, Jing Peng¹, Yang Zhao^{1,2} 

¹Department of Radiology, The Second Hospital of Tianjin Medical University, Tianjin, People's Republic of China; ²Tianjin Institute of Urology, The Second Hospital of Tianjin Medical University, Tianjin, People's Republic of China

*These authors contributed equally to this work

Correspondence: Yang Zhao; Jing Peng, Department of Radiology, The Second Hospital of Tianjin Medical University, Tianjin, 300211, People's Republic of China, Email yang.zhao@tmu.edu.cn; jing.peng@tmu.edu.cn

Purpose: BSA-biom mineralized Gd nanoparticles (Gd@BSA NPs) have been recognized as promising nanoscale MR contrast agents. The aim of this study was to carry out a preclinical evaluation of these NPs in a middle-sized animal model (rabbits).

Methods: New Zealand white rabbits were treated intravenously with Gd@BSA NPs (0.02 mmol Gd/kg) via a clinically-used high-pressure injector, with commercial Gd-diethylene triamine pentaacetate (Gd-DTPA)-injected group as control. Then MR angiography was performed according to the standard clinical protocol with a 3.0-T MR scanner. The SNR and CNR of the main arteries and branches were monitored. Pharmacokinetics and bioclearance were continuously evaluated in blood, urine, and feces. Gd deposition in vital organs was measured by ICP-MS. Weight monitoring, HE staining, and blood biochemical analysis were also performed to comprehensively estimate systemic toxicity.

Results: The ultrasmall Gd@BSA NPs (<6 nm) exhibited high stability and T1 relaxivity. Compared to Gd-DTPA, Gd@BSA NPs demonstrated superior vascular system imaging performance at ultralow doses, especially of the cardiac artery and other main branches, and exhibited a significantly higher SNR and CNR. Notably, the Gd@BSA NPs showed a shorter half-life in blood, less retention in organs, and improved biocompatibility.

Conclusion: The preclinical evaluations here demonstrated that Gd@BSA NPs are promising and advantageous MR CA candidates that can be used at a low dose with excellent MR imaging performance, thus suggesting its further clinical trials and applications.

Keywords: preclinical evaluation, ultralow dose, high-pressure injector, MR angiography

Introduction

Magnetic contrast agents (CAs) are routinely used in 40–50% of all clinical MR examinations.¹ The overwhelming majority of the commercially available CAs for magnetic resonance imaging (MRI) are Gd-based chelators due to their signal brightening effect, high signal-to-noise ratio (SNR) and absence of magnetic susceptibility artifacts.² It has been accepted that Gd CAs could be rapidly excreted after intravenous injection and are thus safe for human use. Unfortunately, recent decades have witnessed increasing reports of the safety concerns after Gd CA exposure, including nephrogenic systemic fibrosis and long-term metal deposition in the body (like brain, kidney, liver and bones), as well as an uncertain association with joint and cognitive symptoms.^{3,4} To address these concerns, a large number of novel CAs have been developed as alternatives to commercial Gd-based chelators,^{5–7} among which protein-biom mineralized Gd CAs have attracted great attention.^{8–11} In particular, the successful application and excellent efficacy of the commercially available paclitaxel-loaded albumin nanosuspension formulation (Abraxane[®]) demonstrates the great clinical prospects of albumin carriers, thus inspiring the synthesis of various protein-based complexes for biomedical applications.^{12,13} In this

context, bovine serum albumin (BSA)-based Gd nanoparticles (Gd@BSA NPs) have been widely investigated by numerous researchers and recognized as a promising MR CA candidate.¹⁴

Gd@BSA NPs are synthesized by protein biomineralization and then stabilized within the template of BSA and have shown great potential for clinical translation. Serum albumins, such as BSA and human serum albumin (HSA), are endogenous substances that are nontoxic, biodegradable, water soluble, and nonimmunogenic.¹⁵ Over the last decade, albumin has been explored as a biotemplate to synthesize metal-containing inorganic NPs.^{16–18} Biomineralization, a bioinspired method in which live organisms produce minerals, is a straightforward, efficient, and environmentally friendly way to fabricate NPs without the use of organic solvents or cross-linking agents.^{19–21} Unlike traditional artificial gadolinium complexes, Gd@BSA NPs have been confirmed by a number of studies to be biocompatible and easy to modify and have high T1 relaxivity,^{22,23} suggesting their potential as clearable novel MR CA candidates.²⁴ However, most of the current research has focused on exploring the characteristics and unique properties of Gd@BSA NPs,^{25–27} but their clinical translation prospects as a promising MR CA candidate have not been fully elucidated. For example, most of the animal models used in previous studies were mice,^{28,29} and their enhanced MR imaging performance has rarely been explored in medium- to large-sized animals. Moreover, comprehensive analyses of their pharmacokinetics, biodistribution, and toxicity are crucial but remains unclear. Furthermore, the CAs reported in previous studies were administered by hand bolus injection, which does not comply with clinically approved medical procedures, namely, high-pressure bolus injection.^{30,31} The nonuniformity in operator experience and injection rates may induce inconsistencies in the pharmacokinetic properties and biodistribution between the experimental and clinical results.³² Therefore, explicit preclinical evidence is indispensable for further clinical applications of Gd@BSA NPs.

In this study, to verify the clinical potential of protein-based CAs, Gd@BSA NPs were synthesized by a biomineralization method and then injected into model rabbits for the first time by a clinically used high-pressure injector for 3.0-T contrast-enhanced MR angiography (CE-MRA) and 3D reconstruction imaging. The prepared Gd@BSA NPs had an ultrasmall particle size (<6 nm), high relaxation rate (r_1 value of $17.987 \text{ mM}^{-1} \text{ s}^{-1}$), and superb stability in pure water and serum. After systematic injection, the MRA images performed with the standard clinical protocol using a clinical 3.0-T MR scanner demonstrated that the prepared Gd@BSA NPs allowed clearer depiction of the anatomical details of the main vessels and their subclass branches, such as cardiac secondary arteries, which are otherwise indistinguishable by enhanced MRA with commercial Gd-DTPA. In particular, the Gd@BSA NP-mediated T1-weighted imaging (T1WI) showed a significantly higher SNR and contrast-to-noise ratio (CNR) than the Gd-DTPA enhanced images, even when the Gd dose in the former was one-fifth that in the latter group. In addition to the excellent imaging performance, dynamic MR imaging also suggested that Gd@BSA NPs were more rapidly cleared by the hepatorenal system, which was consistent with a shorter half-life measured by pharmacokinetic analysis. Moreover, biodistribution analysis showed that Gd@BSA NPs deposited less Gd in the major organs over 14 days, especially in the brain parenchyma, when compared to commercial MR CAs. Furthermore, Gd@BSA NPs demonstrated better biocompatibility in histopathological experiments, blood biochemical tests, and animal body weights, perhaps benefiting from the green chemical synthesis, BSA biomolecular coating, excellent stability, rapid bioclearance, negligible deposition, and reduced dose injected, which was a result of the superior T1 relaxivity. By virtue of their excellent biosafety and MRA performance in medium-sized animals, the Gd@BSA NPs demonstrate great potential for clinical translation, thus providing a viable and advantageous alternative to clinical MRI CAs.

Materials and Methods

Materials and Chemicals

The BSA protein (molecular weights 68KD), $\text{Gd}(\text{NO}_3)_3 \cdot 6\text{H}_2\text{O}$, NaOH, dimethyl sulfoxide and 3-(4,5-Dimethylthiazol-2-yl)-2,5-diphenyl tetrazolium bromide (MTT) were obtained from Aladdin Reagent Co. Ltd. (Shanghai, China) and were of analytical grade or above. Ultrapure water was prepared using a Millipore Simplicity system (Millipore, Bedford, USA). All chemicals were used directly without further purification.

Synthesis of Gd@BSA NPs

According to previous studies, the particle sizes of Gd@BSA NPs vary according to the ratio of BSA/Gd/NaOH.³³ Thus, we chose five BSA/Gd/NaOH molar ratios to synthesize Gd@BSA NPs to optimize the size of the NPs to meet the injection requirements. In brief, BSA was dissolved in 5 mL of water, followed by the rapid addition of Gd(NO₃)₃ solution. Then, NaOH was added to the above mixture, which was stirred overnight at room temperature. Next, the resultant mixture was separated by centrifugation at 10,000 rpm for 15 min to obtain a transparent Gd@BSA NPs solution. Ultrafiltration was further performed with 30 KDa centrifugal filter unit [Amicon Ultra-15 Centrifugal Filter Unit with Ultracel-30 membrane (30 KDa), Millipore] at 5000 rpm for 45 min to remove excess Gd ions in the supernate. These purification procedures were repeated 3 times. Finally, the as-obtained stock solution was stored at 4°C for further use.

Characterization

The high-resolution transmission electron microscopy (HRTEM) images of Gd@BSA NPs were recorded using a JEM-2800 transmission electron microscope (JEOL, Japan) at an accelerating voltage of 200 kV. Then, elemental mapping analysis of the prepared particles was performed by an energy-dispersive X-ray spectroscopy (EDX) detector attached to HRTEM. The hydrodynamic diameters and size distributions of the samples were measured using dynamic light scattering (DLS, Nanozetasizer from Malvern). The absorbance spectra were recorded on the UV-Vis-NIR spectrophotometer (UV2600, Shimadzu, Japan). The crystalline structure and phase purity analysis was performed by X-ray diffraction (XRD) using a Aeris X-ray benchtop diffractometer (Malvern Panalytical, Netherlands).

Measurement of Longitudinal Relaxivity

The atomic Gd contents in the stock solutions of Gd@BSA NPs and Gd-DTPA were quantified by inductively coupled plasma–mass spectrometry (ICP–MS, 8600MD, YS EXT, China). Then, the stock solutions were diluted with ultrapure water to obtain different concentrations of Gd. Next, these samples were placed into a clinic 3.0-T scanner (MAGNETOM Vida, Siemens Healthineers, Germany) equipped with a 32-channel phased array head coil at the room temperature. A fast T1-mapping sequence was performed to measure the longitudinal relaxation times (T1) under the following parameters: TR/TE = 5.2/2.4 ms; Field of View = 225×280 mm²; Slice Thickness = 2 mm, Spacing = 0.3 mm, Matrix = 256×144, Number of Averages = 6, Number of Repetitions = 1, Flip Angle = 3, 15, and 16°. The r1 relaxivity values were determined by the slope of the curve fitting 1/T1 relaxation time (s⁻¹) as a function of the Gd concentration (mM⁻¹).

In vitro Cytotoxicity

The human cervical cancer cells (HeLa) and mouse mononuclear macrophage leukemia cells (RAW264.7) were obtained from the Wuhan Punosai Life Technology Co, Ltd, China. HeLa and RAW264.7 cells were cultivated in DMEM (Gibco, Carlsbad, CA, USA) containing 2 mM L-glutamine and 10% fetal bovine serum (FBS, Gibco, Carlsbad, CA, USA). Cell viability was determined by MTT assay. In short, HeLa and RAW264.7 cells were inoculated in 96-well plates (2000 cells/well). Then, the culture medium was replaced with fresh medium containing 200 μL of Gd@BSA NPs at various concentrations. After 24 h of incubation, the cells were washed with PBS, followed by treatment with MTT (5.0 mg/mL) in pure water for 2 h. The cell culture medium was removed, and 150 μL of dimethyl sulfoxide was added to each well. The optical density (OD) of each well was measured at 490 nm.

$$\text{Cell viability(\%)} = (\text{mean OD of the selected treatment group} / \text{mean OD of the control group}) \times 100$$

Model Animals

New Zealand white rabbits (3.0–3.5 kg of body weight) were used as the model animals. The rabbits were kept in the Animals Housing Facility, Tianjin University of Traditional Chinese Medicine. They were housed at a constant temperature and provided with commercial feed rabbit chow ad libitum and water. Animal experiments were carried out under protocols approved by the institutional animal care and use committees of Tianjin University of Traditional

Chinese Medicine (TCM-LAEC2023048). The animal use and welfare complied with the principle of the 3Rs for animal testing and research.

MRI Scanning and Image Reconstruction

MR imaging was performed using a 3.0-T clinic MR system (Discovery 750, GE Healthcare, USA) with an 8-channel phased array spine coil. Prior to all procedures, rabbits were anesthetized by intraperitoneal (IP) injection of pentobarbital sodium (50 mg/kg). A 26-gauge intravenous cannula was inserted into the marginal ear vein. Then, the anesthetized rabbits were placed in the supine position on a spinal coil in the isocenter of the magnet. Next, the prepared Gd@BSA NPs (0.02 mmol Gd/kg in pure water) or commercial Gd-DTPA (0.1 mmol Gd/kg) were automatically injected into the rabbits with a clinically used high-pressure injector (Medrad Spectris Solaris EP, Bayer, Germany) linked with the indwelling cannula, followed by an additional 5 mL of saline at the same flow rate. The high-pressure syringe was equipped with contrast A and B cartridges. The former was used for the injection of the CA (Gd@BSA NPs or Gd-DTPA), while the latter was exploited to push saline into the heart and prevent intravascular clotting in the punctured vein to keep it open. The injection rate (0.2 mL/s) and dose (3 mL) were set in advance before the enhancement scan after successful puncture.

T1WI and fat-saturated 3D gradient echo imaging were performed at consecutive time points postinjection. The detailed imaging parameters are as follows: TR/TE = 400/10 ms, 256×256 matrices, slices = 3, thickness = 2 mm, averages = 4, and FOV = 60×60. The obtained imaging data were subsequently transferred to a clinical workstation (AW4.6, GE Healthcare) for further image analysis and postprocessing. Subvolume maximum intensity projection (MIP) and volume rendering images were reconstructed by the workstation to display the large vessels and their major branches.

Image Analysis

The enhanced T1-weighted images obtained from the above experiments were quantitatively analyzed. Regions of interest (ROIs) were drawn in the cardiac artery, thoracic aorta, aortic arch, abdominal, renal and iliac arteries, and their MR signal intensity was measured.

SNRs were calculated by the following equation: $SNR = SI_{ROIs}/SD_{noises}$, where SI_{ROIs} represents the average signal intensity of the ROIs in the T1-weighted MR images and SD_{noises} represents the standard deviation of background signal intensity.

The CNRs in the MR images were calculated using the following equation: $CNR = (SI_{tumor} - SI_{muscle})/SI_{noises}$, where SI indicates the signal intensity, and the noise was estimated from the air background.

Pharmacokinetics, Biodistribution, and Excretion

Two milliliters of Gd@BSA NPs (0.1 mmol Gd/kg) or Gd-DTPA (0.1 mmol Gd/kg) was intravenously injected into rabbits ($n=3$) via the marginal ear veins. Blood samples of 100–200 μ L were collected at scheduled time points. The plasma concentrations of Gd were determined by ICP–MS.

Two weeks after contrast material injection, the rabbits were sacrificed, and their hearts, livers, spleens, lungs, and kidneys were extracted and weighed. Then, the collected organs were pounded into pieces by mortar and digested in 5% nitric acid for 14 days. After filtration, the atomic Gd concentration in each filtrate was quantified by ICP–MS. The biodistribution of the Gd@BSA NPs in the various organs of the rabbits was calculated, and the results are presented as the percentage of injected dose per gram of tissue (%ID/g).

To study the excretion profiles of the prepared nanocomposites, rabbits were kept in a metabolic cage after intravenous injection of Gd@BSA NPs. Their urine and feces were collected, digested with concentrated nitric acid, and finally the Gd contents were determined by ICP–MS. The pharmacokinetic parameters were obtained from the pharmacokinetic software DAS 2.0 (Drug and Statistics Version 2.0).

In vivo Toxicity

The in vivo systemic toxicity of Gd@BSA NPs was comprehensively evaluated by body weight monitoring, hematoxylin-eosin (HE) staining, and blood biochemistry analysis. Gd@BSA NPs (0.1 mmol Gd/kg) were injected intravenously,

while rabbits treated with Gd-DTPA at the standard dose (0.1 mmol Gd/kg) were used as controls. The body weights of the rabbits were monitored every other day.

Approximately 0.6 mL of blood was collected at various time points after injection from 3 rabbits per group at each time point. Routine blood analysis and biochemical analysis were performed using a hematology analyzer (KT-6200, Genrui-bio, China) and a fully automatic chemistry analyzer (FUJI DRI-CHEM NX500iVC, FUJIFILM, Japan). Then, the rabbits were euthanized on day 14. The heart, liver, spleen, lung, and kidney were dissected, fixed in 10% neutral buffered formalin, routinely processed into paraffin, sectioned at 5 μm , stained with HE, and examined with a digital microscope.

Statistical Analysis

All statistical analyses were performed with GraphPad Prism v.8.0.2 (GraphPad Software). All data are presented as the mean \pm standard deviation. Comparisons between two groups were conducted with Student's *t*-test (* $P < 0.05$, ** $P < 0.01$, *** $P < 0.001$, and **** $P < 0.0001$).

Results

Synthesis and Characterization of Gd@BSA NPs

Gd@BSA NPs were synthesized by a one-step biomineralization method. Here, we attempted to adjust the sizes of the Gd@BSA NPs by varying the feeding amounts of Gd, BSA, and NaOH. DLS showed that the average diameters of the synthesized Gd@BSA NPs ranged from 5.05 to 29.00 nm (Figure S1a–f). The smallest hydrated particle size that could be stabilized below 6 nm was generated using 150 mg of BSA, 1.00 mL of Gd(NO₃)₃ solution (0.03 M) and 300 μL of NaOH (1.00 M). The TEM results showed that the prepared ultrasmall Gd@BSA NPs were round, monodispersed and uniform. Their average size measured by TEM was 4.98 nm, which agreed well with the DLS results (Figure 1a), and their zeta potential was -27.97 mV (Figure S2). In addition, the ultraviolet–visible (UV–Vis) spectra of Gd@BSA NPs exhibited an absorbance band at 280 nm originating from the protein template (Figure 1b). The X-ray diffraction (XRD) pattern of Gd@BSA NPs showed characteristic peaks on crystal planes of (100) and (101), which roughly matched the standard card JCPDS: 24–0430 for Gd₂O₃, further confirming the successful formation of Gd₂O₃ in Gd@BSA NPs (Figure S3). In addition, the EDX spectra and elemental analysis were obtained to study the elemental compositions and distributions of Gd@BSA NPs (Figure 1c and d). The carbon (C), nitrogen (N), oxygen (O), sulfur (S), and gadolinium (Gd) elements were detected within Gd@BSA NPs, while Gd was uniformly distributed in the BSA template.

Stability of Gd@BSA NPs

We characterized Gd@BSA NPs in different media by DLS and TEM. TEM analysis provided information on the size, shape and aggregation of the NPs after incubation. The Gd@BSA NPs maintained a uniform dispersion for 2 weeks after incubation in ultrapure water (Figure 1e) and FBS (Figure 1f). In addition, the sizes of the Gd@BSA NPs in ultrapure water and FBS solution were not significantly different from their initial values (Figure S4a and b), which was consistent with the TEM results. Overall, the stability experiments showed that ultrapure water and serum could be considered good media due to their ability to maintain a stable size and shape of the Gd@BSA NPs.

Relaxometry of Gd@BSA NPs

To evaluate the T1 relaxation properties of Gd@BSA NPs, in vitro T1WI of Gd@BSA NP solutions was carried out on a 3.0-T clinical MR scanner (Figure 1g and h). As shown in Figure 1h, the measured T1 relaxivity value (r_1) of the Gd@BSA NPs was $17.987 \text{ mM}^{-1}\text{s}^{-1}$ on a Gd basis, which was significantly higher than that of the clinically used Gd-DTPA ($5.737 \text{ mM}^{-1}\text{s}^{-1}$).

MRI and MRA Performance of NPs Injected Rabbits

Based on the remarkable T1 contrast-enhancing capability of Gd@BSA NPs in vitro, we next investigated the in vivo vascular enhancement performance of the prepared Gd@BSA NPs. The in vitro stability results (Figure 1e and f)

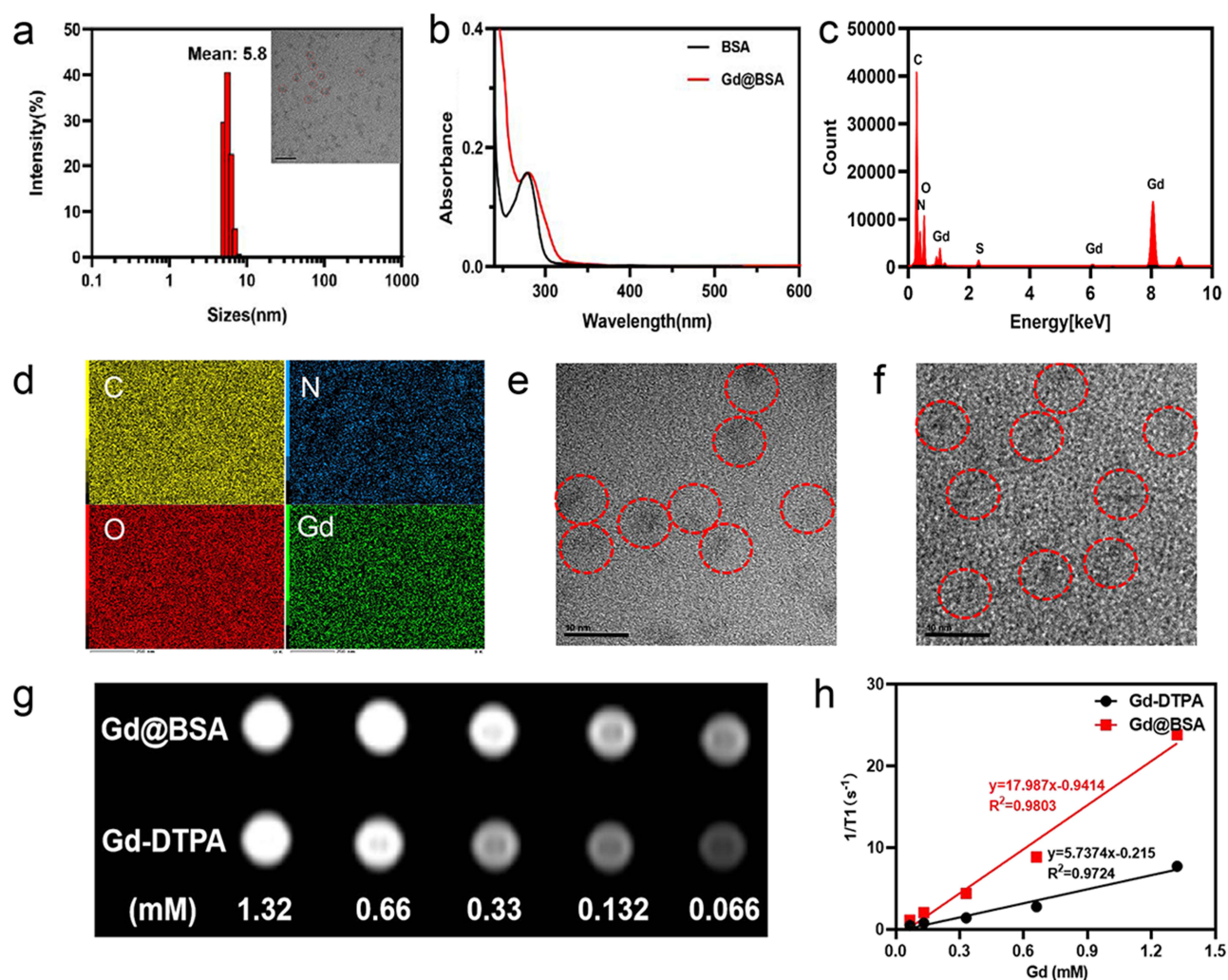


Figure 1 Characterization of Gd@BSA NPs. (a) Hydrodynamic diameter of Gd@BSA NPs determined by DLS. And TEM image of Gd@BSA NPs; red dotted circles indicate nanoparticles. (b) UV-vis absorption spectra of BSA and Gd@BSA NPs. (c and d) Energy-dispersive X-ray spectroscopy (EDX) and elemental analysis performed on Gd@BSA NPs. EDX spectrum, and corresponding elemental mapping for nitrogen (N), oxygen (O), sulfur (S), gadolinium (Gd). (e and f) TEM images of Gd@BSA NPs in H₂O and FBS, respectively. (Red circles: locations of Gd@BSA NPs). (g) T1-weighted MR images of Gd@BSA NPs and Gd-DTPA at different Gd concentrations. (h) Analysis of the longitudinal relaxation rates r_1 ($1/T_1$) of Gd@BSA NPs and Gd-DTPA. T1 relativity was calculated from the slopes of the best fit lines of the experimental data.

described above showed that ultrapure water and FBS were ideal media for Gd@BSA NPs. Therefore, we dissolved the prepared NPs in pure water for injection (Figure S5). Briefly, 3.00 mL of Gd@BSA NPs (0.02 mmol Gd/kg) was automatically injected into the marginal ear veins of rabbits via a clinically used high-pressure injector at a flow rate of 0.20 mL/s, followed by 5.00 mL of saline at the same flow rate. Then, MR angiography was performed using a clinical 3.0-T MR scanner system. Rabbits treated with commercial Gd-DTPA (0.10 mmol Gd/kg) were used as the control.

In the postcontrast images, the Gd@BSA NPs showed good contrast of the vessel lumen, and the major aortic branches were clearly visible (Figure 2a). The signals of the aortic arch, carotid artery, descending thoracic aorta, abdominal aorta, bilateral iliac arteries, and renal arteries were significantly enhanced, as shown in Figure 2b, c and e. Although there was no significant difference in the signal intensities of the large vessels (such as the descending thoracic aorta and abdominal aorta) between the Gd@BSA NP group and the Gd-DTPA group, clear bilateral iliac and renal arteries could be seen in only the former group but were indistinguishable in the Gd-DTPA-enhanced MRA. (Figures 2d and S6). More specifically, MRA using Gd@BSA NPs provided superior visualization of the cardiac vessels and their secondary and tertiary branches compared with the images obtained with the commercial CA Gd-DTPA (Figures 2f and g and S7). This phenomenon was considered to result from the thinness of the bilateral iliac and renal arteries as well as the very small amount of contrast

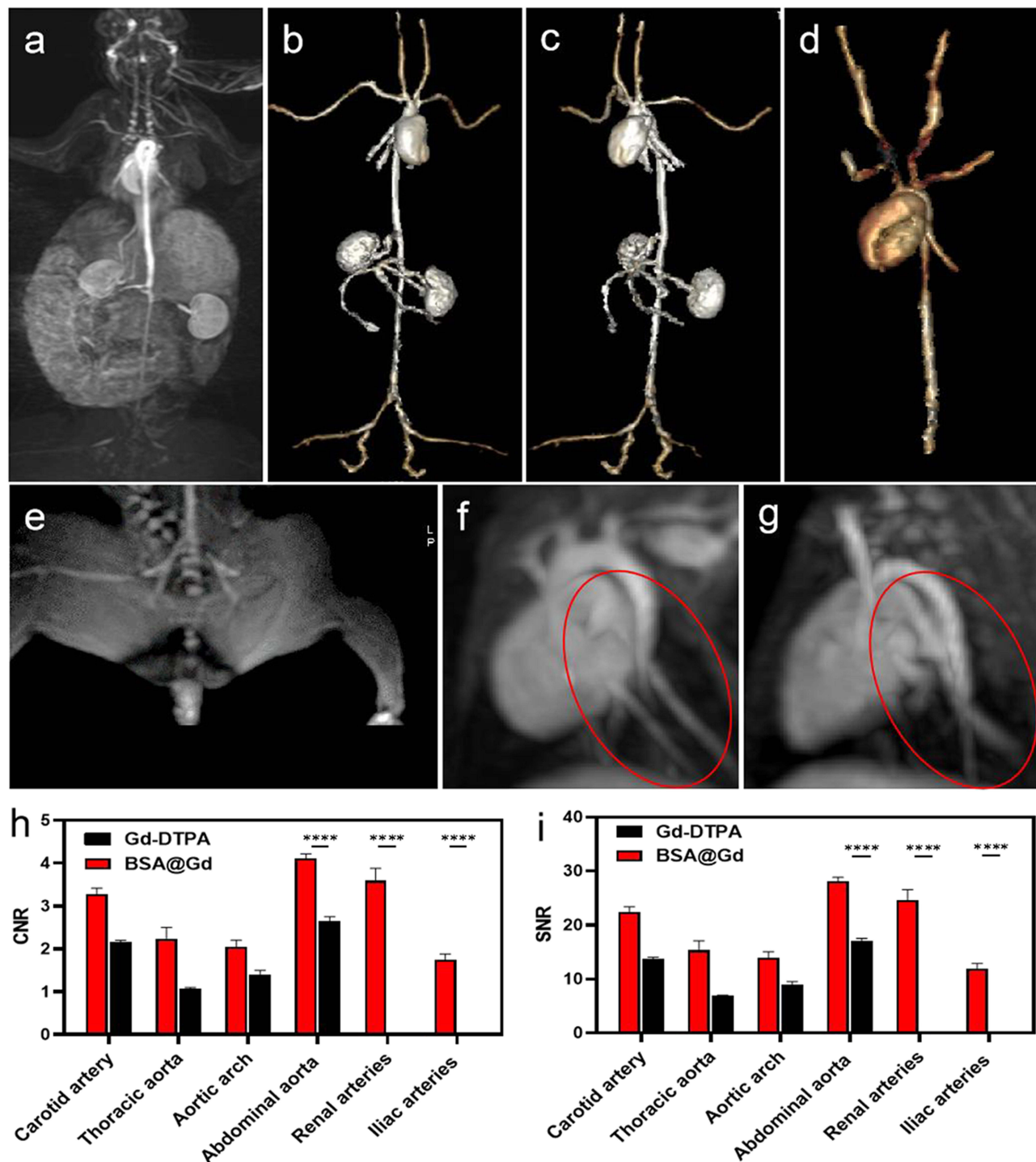


Figure 2 In vivo MR angiography of the Gd@BSA NP contrast agent. (a) Coronal maximum intensity projection (MIP) images and (b and c) 3D reconstructed angiogram of rabbits after injection with Gd@BSA NPs. (d) 3D reconstructed angiogram of rabbits after injection with Gd-DTPA NPs. (e) Angiographic images of iliac arteries and branches of rabbits after injection with Gd@BSA NPs. (f and g) Angiographic images of the secondary and tertiary vessels (red circles) in rabbit hearts after intravenous injection of Gd@BSA NPs and Gd-DTPA. (h and i) Quantitative analysis of the abovementioned vessels. **** $P < 0.0001$.

agent filling the distal vessels, so that only the Gd@BSA NPs with a high relaxation rate could clearly depict the small vessels at the ultralow dose administered. In addition, as the injection speed of the clinically used high-pressure injector was much greater and more stable than those of hand bolus injection, multiphase contrast-enhanced MRI could be achieved, including the arterial, venous, and excretory phases.

SNR and CNR of NPs Injected Rabbits

In this study, evaluation of the image quality and the presence of artifacts were examined by three radiologists with more than 15 years of clinical experience. Three observers manually segmented six vessels, the carotid artery, thoracic aorta, aortic arch, abdominal aorta, renal artery and iliac artery, and measured the signal intensities of the vessels by enhanced T1WI. [Figure 2h](#) and [i](#) shows the SNRs and CNRs of the main arteries and branches. Quantitative image analysis of the enhanced T1WI scans acquired with Gd@BSA NPs demonstrated significantly higher SNRs and CNRs in the vessels, especially in slender vessels such as the bilateral iliac and renal arteries. In addition, the time-signal intensity curves revealed that the remarkable enhancement observed in the Gd@BSA NP group could be maintained 4 times longer in the arterial phase than that in the Gd-DTPA group ([Figure S8](#)). These results demonstrated that Gd@BSA NPs had great potential for MR angiography as a T1-positive contrast agent.

Mixed Renal and Hepatobiliary Metabolism

Unambiguous and efficient excretion of NPs is of fundamental importance for in vivo biomedical applications. There are two primary routes by which NPs are cleared from the body: renal filtration with excretion in urine and hepatobiliary processing with excretion in bile. Commercially available Gd chelators such as Gd-DTPA are predominantly excreted through the kidneys and their use is not advised in patients with renal dysfunction. Therefore, novel paramagnetic NPs cleared by the hepatobiliary system may help alleviate the burden of CA metabolism on the kidney.

Herein, the signal intensity changes in the hepatobiliary and urinary systems were dynamically monitored to noninvasively determine the transit and excretion of the injected Gd@BSA NPs. [Figure 3a](#) shows coronal T1-weighted images before Gd@BSA NP injection and 10 min, 30 min, 1 h, 2 h and 24 h after injection. After Gd@BSA NP injection, the signals in the bilateral renal pelvis and bladder of the rabbits were significantly enhanced and weakened over time as observed in the dynamic images. [Figure 3b](#) displays optimal enhancement of the renal cortex, parenchyma, and collecting systems, corresponding to the appearance of the NPs in the clinically used corticomedullary, nephrogenic, and excretory phases. These data indicated that the use of the prepared Gd@BSA NPs was promising for 3-phase contrast-enhanced renal imaging. Moreover, the dynamic changes in liver were also monitored. Here, a slight enhancement was found at 10 min postinjection, and subsequently, the signal in the gallbladder was significantly enhanced at 0.5 h ([Figure 3c](#)). Thereafter, these signals gradually diminished. Twenty-four hours later, the liver and kidney signals were almost completely restored. These results suggested that Gd@BSA NPs were cleared by the kidney and hepatobiliary system.

Furthermore, animal urine and feces were collected and quantitatively analyzed by ICP-MS. The entire metabolic process of the Gd@BSA NPs at different times after intravenous administration is shown in [Figure 4a](#), and the results revealed that the majority (64.34%) of the Gd@BSA NPs were excreted in the urine within 7 days, with 30.39% of the Gd excluded through the feces ([Table S1](#)). These results suggested that Gd@BSA NPs could be almost completely cleared from the body through the mixed renal and hepatobiliary system (94.73% in total).

Pharmacokinetics and Deposition on NPs-Injected Rabbits

To clarify how Gd@BSA NPs exist in the blood circulation, we then determined the pharmacokinetic profile of these NPs in rabbits. For this purpose, Gd@BSA NPs at the clinically used Gd dose (0.10 mmol/kg) were administered to 3 rabbits by intravenous injection, and Gd-DTPA at the same dose of Gd was injected into the control rabbits. Plasma concentration-time curves ($n = 3$) were constructed as shown in [Figure 4b](#) and indicate that the elimination half-lives ($t_{1/2}$ values) of Gd@BSA NPs and Gd-DTPA in plasma were 79.17 ± 14.17 min and 96.33 ± 20.61 min, respectively. This result showed that Gd@BSA NPs shortened the circulation time of Gd in the blood compared to Gd-DTPA.

Considering that the long retention time of Gd-DTPA in circulation may be associated with uncertain safety issues, we further evaluated the deposition and bioclearance of Gd@BSA NPs by measuring the content of Gd in different rabbit organs (heart, liver, spleen, lung and kidney) by ICP-MS analysis. As shown in [Figure 4c](#), 14 days after intravenous injection of Gd@BSA NPs, the residual amounts of Gd in the kidney, brain parenchyma, lung, spleen and heart were significantly less than that in the Gd-DTPA-treated group. However, the residual amount of Gd in the livers of the rabbits

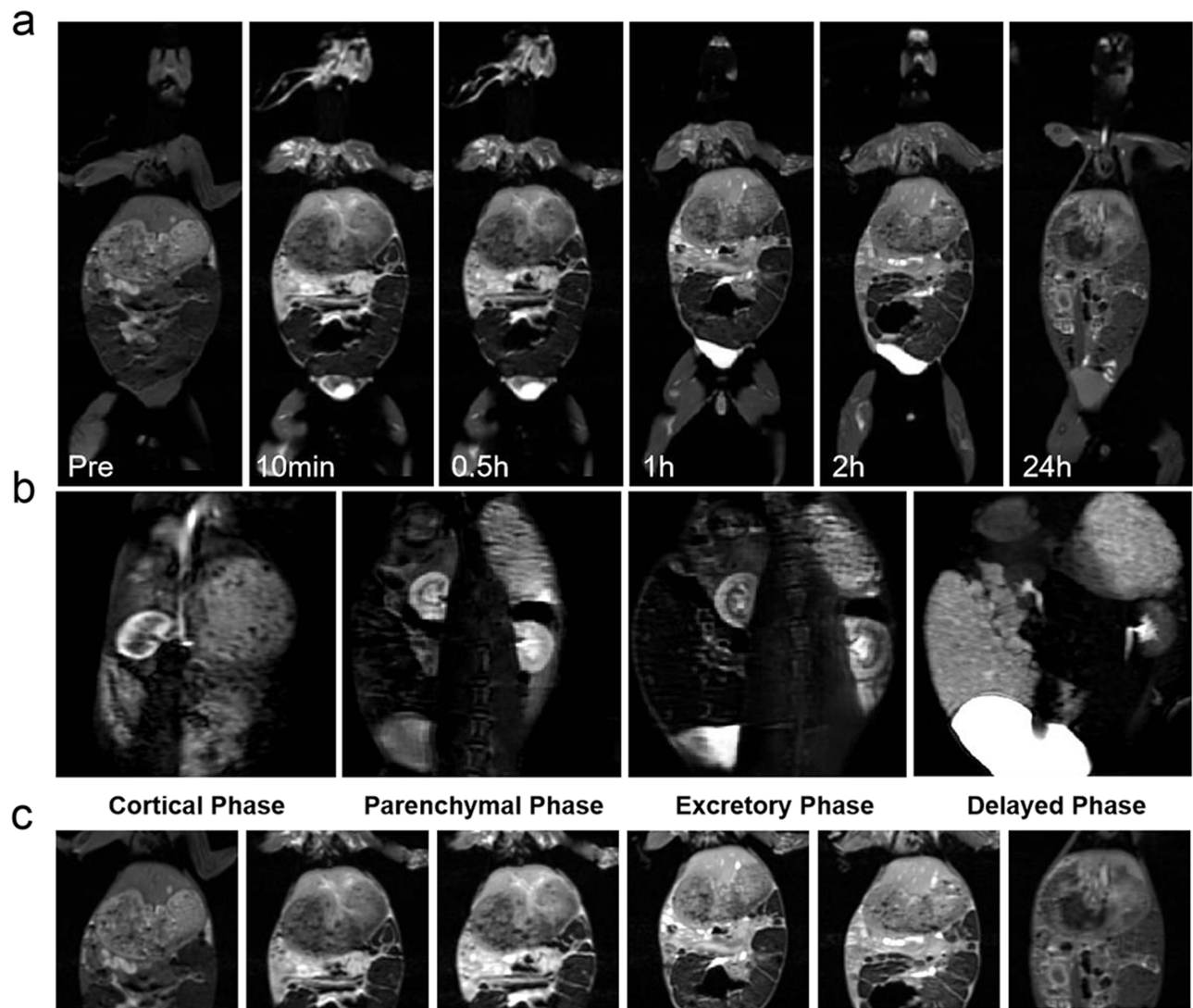


Figure 3 In vivo postcontrast MR images of the Gd@BSA NPs over time. (a) Coronal T1-weighted MR images acquired from rabbits injected with Gd@BSA NPs at a Gd dose of 0.02 mmol/kg body weight. Precontrast and 10 min, 0.5 h, 1 h, 2 h and 24 h postcontrast images are shown from left to right. (b) Dynamic multiphase enhanced MR images of the kidneys from rabbits administered Gd@BSA NPs. (c) T1-weighted MR images of the livers from rabbits injected with Gd@BSA NPs.

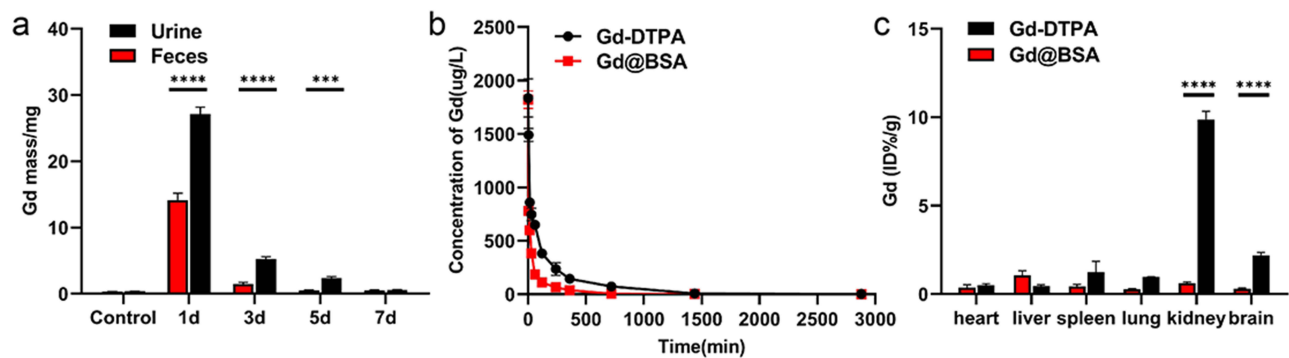


Figure 4 In vivo pharmacokinetics and biodistribution of the Gd@BSA NPs. (a) The mass of Gd detected in feces and urine at different time points after intravenous injection of Gd@BSA NPs (0.1 mmol/kg). (b) Concentration-time profiles of Gd in blood after rabbits were intravenously injected with Gd@BSA NPs. (c) Biodistribution of the Gd@BSA NPs in the major organs of the rabbits 14 days after intravenous injection. Each column represents the mean±SD. ***P<0.001, ****P<0.0001.

in the Gd@BSA NP group was slightly higher than that in the Gd-DTPA-treated group, which may be attributed to the mixed renal and hepatobiliary metabolism of the prepared NPs. Overall, for all rabbits, the total Gd retention after Gd@BSA NP administration in vivo was significantly less than that after treatment with Gd-DTPA, which is consistent with the elimination half-life results described above. These data suggested that the bioclearance of Gd@BSA NPs was superior to that of the clinically used Gd-DTPA, which could avoid the safety concerns of Gd CA exposure.

Systematic Toxicology on NPs-Injected Rabbits

The cytotoxicity of Gd@BSA NPs was evaluated by standard cellular MTT assay. After incubation with Gd@BSA NPs at different concentrations (Figures S9 and S10), human cervical carcinoma cells (HeLa cells) and murine macrophages (RAW264.7 cells) had no significant drop in viability. Even at 1100 $\mu\text{g/mL}$ NPs, the relative viability remained above 90%, demonstrating the negligible cytotoxicity of Gd@BSA NPs.

To further investigate the systematic biocompatibility of Gd@BSA NPs in vivo, clinical markers, including blood biochemical analysis, histological changes, and body weight changes, were investigated comprehensively (Figures 5 and S11). For blood biochemistry assays, the blood samples from the rabbits treated with Gd@BSA NPs were collected at the

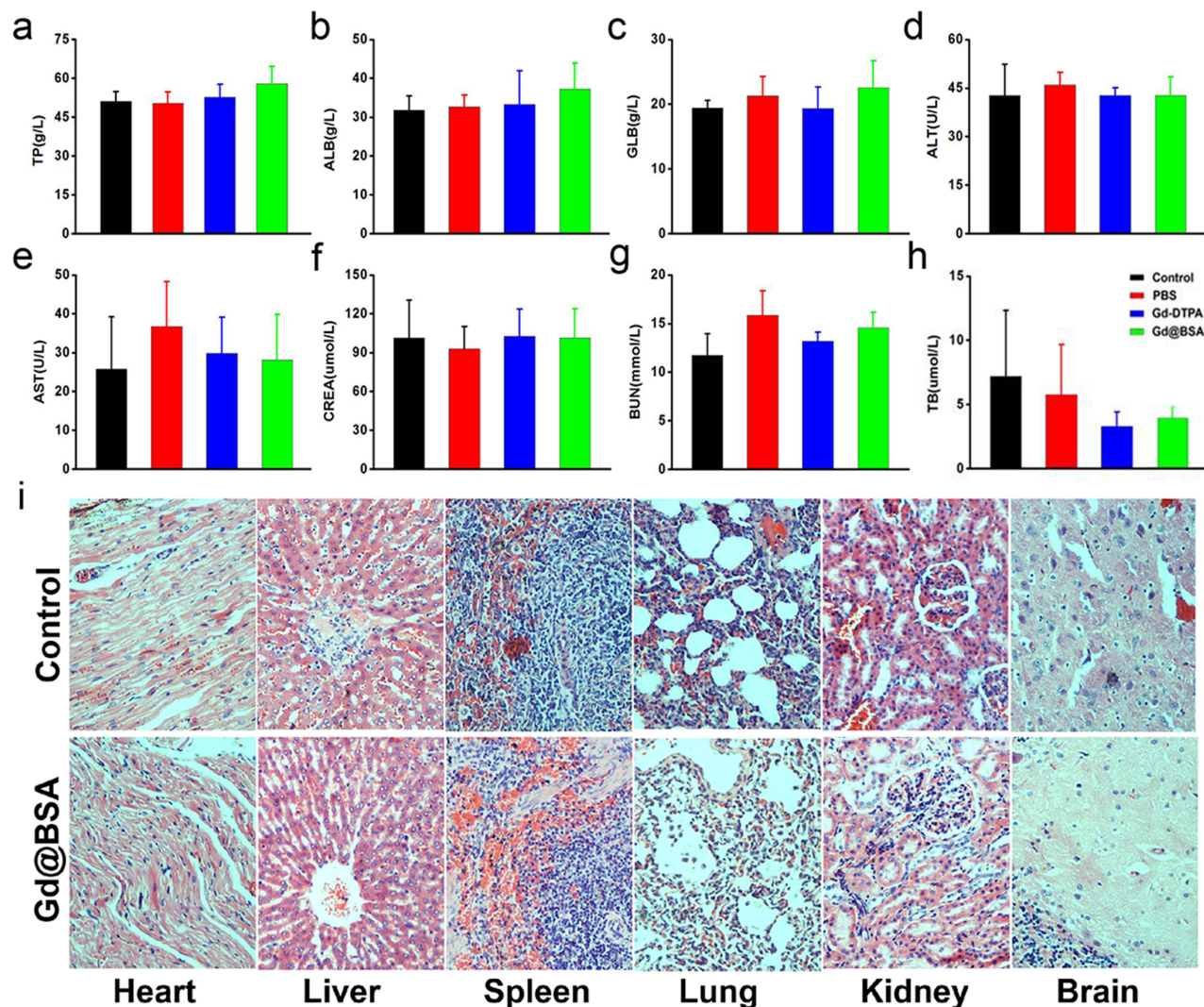


Figure 5 In vivo biosafety of Gd@BSA NPs. (a–h) Blood biochemical indicators from the rabbits preinjection and at 1 day or 14 days postinjection of Gd-DTPA or Gd@BSA NPs. (i) HE-stained images of the major organs from untreated rabbits (control) and rabbits injected with Gd@BSA NPs after 14 days.

Abbreviations: TP, total protein; ALB, albumin; GLB, serum globulin; ALT, alanine aminotransferase; AST, aspartate aminotransferase; CREA, creatinine; BUN, urea nitrogen; TB, total bilirubin.

Table 1 Hematology Data from Rabbits Injected with Gd@BSA NPs (n = 3)

	Pre	5 min	15 min	30 min	1h	2h	4h	6h	1d	7d	14d
WBC($10^9/L$)	7.46	5.64	6.00	4.26	5.76	4.02	4.62	7.05	11.15	9.24	10.73
RBC($10^{12}/L$)	4.99	5.09	5.389	4.49	5.08	5.38	4.89	4.49	3.93	3.18	3.95
PLT($10^9/L$)	237.60	198.80	138.67	182.33	176.40	122.40	139.60	135.00	131.29	489.40	219.33
HGB(g/L)	338.60	332.00	333.20	333.80	331.80	330.60	345.67	342.67	360.86	336.60	317.67
NE($10^9/L$)	5.00	3.76	4.42	3.08	3.68	2.62	4.00	6.25	7.00	5.86	9.03

scheduled time points (preinjection, 1 day and 14 days postinjection). All biochemical indicators of liver function (TP, ALB, ALT, AST), kidney function (CREA, BUN), and serum globulin (GLB) showed no significant difference from the control group treated with Gd-DTPA (Figure 5a–h). In terms of routine blood tests, red blood cell (RBC), white blood cell (WBC), hemoglobin (HGB), and platelet (PLT) counts were measured at different time points (preinjection, 5min, 15min, 30min, 1h, 2h, 4h, 6h, 12h, 1d, 7d, 14d postinjection, Table 1). During the observation period, all of these parameters in the Gd@BSA NP group were within the reference (normal) range and showed little change compared to the preinjection period. Comparatively, the above indexes in the Gd-DTPA group showed relatively larger changes, but eventually returned to the original levels (Table S2). Moreover, pathological analysis showed that 14 days of Gd@BSA NP exposure elicited no significant histological changes in the susceptible organs (heart, liver, spleen, lung, kidney, and brain) compared with Gd-DTPA (Figure 5i). Moreover, rabbits injected with Gd@BSA NPs exhibited no abnormal body weight changes or sudden death during the 14 days of observation (Figure S11). All of the above results demonstrated that the Gd@BSA NPs possessed excellent biocompatibility *in vivo*, potentially due to the green chemical synthesis, BSA biomolecular coating, excellent stability, rapid bioclearance, negligible deposition, and ultralow dose injected, which was a result of the superior T1 relaxivity.

Discussion

In this work, we performed a comprehensively preclinical evaluation of Gd@BSA NPs by using the medium-sized animal models of rabbits, and thus provided further evidence for their clinical translation potential. Because of the protein-based biomineralization synthesis method as previously reported,^{34–36} ultra-small Gd@BSA NPs with a hydrodynamic diameter of <6 nm were successfully prepared by adjusting the feeding molar ratio of Gd/BSA as well as the pH environment in the reaction. The as-prepared Gd@BSA NPs exhibited excellent stability and T1 relaxivity, which were beneficial to their further biomedical applications. Different from the previous researches that used small animal models with nonclinical administration versus humans undergoing clinical procedures,^{28,29} we first investigated the *in vivo* performance of Gd@BSA NPs in medium-sized rabbits via the clinically-used high-pressure bolus injection method. By exploiting the clinical MR scanning protocol, our findings demonstrated that the Gd@BSA NPs could be regarded as a potentially viable and advantageous alternative to gadolinium-based contrast agents (GBCAs). The prepared Gd@BSA NPs exhibited good MRI and MRA imaging performance with a high SNR and CNR, excellent pharmacokinetics, thorough clearance, low dispersion, and extreme biocompatibility.

In this study, we achieved excellent enhanced MRI with an ultralow dose of CA. Image analysis demonstrated explicit traditional T1WI by the prepared Gd@BSA NPs with a significantly higher SNR and CNR and 3D reconstruction vascular imaging *in vivo* while also showing advantages in visualizing the cardiac vascular branches compared with commercial MR CAs, even when the Gd dose from the NPs was one-fifth that of Gd-DTPA. Moreover, the high SNRs and CNRs of the vessels (enhanced T1WI) in the clinically relevant 3.0-T MRI field were the main contributors to the high T1 relaxivity of the Gd@BSA NPs. In addition, in the postcontrast vascular enhancement images, the Gd@BSA NPs showed excellent contrast enhancement of the major aortic branches, such as the carotid, renal, and iliac arteries. Furthermore, the high signal enhancement by Gd@BSA NPs allowed easy segmentation and extraction of the vessel tree from the 3D reconstructed angiogram. These results indicated that low doses of Gd@BSA NPs could allow a depiction of the anatomical details of small vessels that is clearer than that given by commercial CAs. For example, MRA with Gd@BSA NPs provided better visualization of the cardiac vessels and their tertiary branches, which were otherwise

indistinguishable by enhanced MRA with commercial Gd-DTPA. These advantages of the Gd@BSA NPs in visualizing vascular systems provides a strong rationale for their further preclinical investigation in vascular disease imaging.

Experimentally, blood pool imaging is usually regarded as magnetic resonance vessel imaging.^{37–39} However, blood pool imaging is almost always performed by hand bolus injection, with which the injection rate is limited, allowing the imaging time to be extended far beyond the short arterial first-pass phase. Therefore, most blood pool images are mixed images of the arterial and venous phases, which is different from clinical MR angiography and cannot be used for further clinical applications. In addition, the speed and volume of the contrast agent that reaches the organs and tissues are inconsistent after high-pressure injection and manual pushing, resulting in the inconsistent display of vascular details, biological distribution and metabolism.⁴⁰ Therefore, when using hand bolus injection, the experimental results could not truly reflect the clinical conditions. Due to these limitations, blood pool agents are not currently used in clinical practice. In the present study, we tried for the first time to inject Gd@BSA NPs into the marginal ear vein of rabbits for MRA using a high-pressure syringe, which allows for uniform CA injection in a short period of time with the addition of saline, thus maximizing the speed, uniformity, and degree of mixing of the contrast agent into the blood circulation. In addition, our preclinical experiment achieved pure arterial phase scanning MRA. These results indicate that we can use nanoscale magnetic resonance contrast agents (Gd@BSA NPs) for multiphase MR vascular examinations, such as MRA and magnetic resonance venography (MRV), to diagnose arteriovenous stenosis, malformations and other diseases.

In this study, dynamic magnetic resonance imaging revealed rapid blood clearance and mixed renal and hepatobiliary elimination of Gd@BSA NPs, which was consistent with the much shorter half-life measured by pharmacokinetic analysis. Moreover, due to injection by a high-pressure syringe similar to that performed in medical procedures, long-term tracing of Gd@BSA NPs at a clinical dose in vivo was achieved. The results revealed that there were few NP residues in the major organs after 14 days, especially in the brain parenchyma, where recent decades have witnessed an increase in the number of reports of the long-term deposition of Gd CAs, which may be attributed to their stability in serum. In contrast, according to previous reports, Gd-DTPA was found to accumulate significantly in the brain and kidney, leading to cerebral Gd deposition and renal organ failure, which is consistent with the pharmacokinetic results. Therefore, Gd@BSA NPs, a nanoscale MR CA, have NP properties, better pharmacokinetic characteristics, a shorter half-life, a lower application dose, and faster drug metabolism than commercial CAs. Specifically, based on the pharmacokinetics and bioclearance of the CA in our study, the outcomes obtained with this injection method are closer to the clinical conditions. Therefore, this preclinical study and the findings herein offer the possibility of the clinical translation of Gd@BSA NPs.

The biosafety of contrast agents is crucial for their clinical translation.^{41,42} In our preclinical study in a medium-sized animal model, histological examination showed that the major organs had no appreciable pathological lesions at 14 days. The blood indicators showed that the Gd@BSA NPs had no deleterious effects on liver or kidney function. All these data demonstrated that Gd@BSA NPs had good biocompatibility and biosafety. In the future, when using low doses of Gd@BSA NPs, we anticipate even greater human safety. This translational study, therefore, has the potential to provide a foundation for a promising nanoscale contrast agent for enhanced MRI and MRA, where it has been acknowledged that the options for CAs are limited.

Conclusion

In summary, this study that exactly mimics the clinical MR scanning protocol could provide uniform, repeatable, and convincing evidence to support the clinical translation potential of Gd@BSA NPs. According to our results, Gd@BSA NPs synthesized by biomineralization method, exhibited high stability and T1 relaxivity. When administrated into the middle-sized animal models via our defined high-pressure pure water bolus injection condition, Gd@BSA NPs displayed superior tissue and vascular enhancement effects over the commercial Gd-DTPA, especially of the cardiac artery and other main branches, and showed a short half-life in blood, rapid clearance, little retention, and improved biocompatibility. This preclinical evaluation study demonstrated that Gd@BSA NPs were a promising, bio-friendly, and efficient nanoscale MR CA candidate that required a low dose but shows excellent MR imaging performance, attributing which are expected for further clinical trials and applications.

Abbreviations

CAs, magnetic contrast agents; MRI, magnetic resonance imaging; SNR, signal-to-noise ratio; HAS, human serum albumin; CE-MRA, contrast-enhanced MR angiography; T1WI, t1-weighted imaging; CNR, contrast-to-noise ratio; TEM, transmission electron microscopy; DLS, dynamic light scattering; ICP-MS, inductively coupled plasma-mass spectrometry; FBS, fetal bovine serum; OD, optical density; IP, intraperitoneal; ROIs, regions of interest; HE, hematoxylin-eosin; UV-Vis, ultraviolet-visible; RBC, red blood cell; WBC, white blood cell; HGB, hemoglobin; PLT, platelet; GBCAs, gadolinium-based contrast agents; TP, total protein; ALB, albumin; GLB, globulin; ALT, alanine aminotransferase; AST, aspartate aminotransferase; CREA, creatinine; BUN, blood urea nitrogen; TB, total bilirubin.

Acknowledgments

This work was supported by the National Natural Science Foundation of China (Nos. 82272804, 91959114, 81872106), the Natural Science Foundation of Tianjin (No. 19JCZDJC33900, 20JCJQJC00270, 22JCQNJC01700), the Scientific and Technological Research Program of Tianjin Municipal Education Commission (No. 2019ZD025), the Scientific and Technological Research Program of Tianjin Health Commission (No. TJWJ2022XK015), the Medical Key Discipline Programme of Tianjin Municipal Healthcare Commission (TJYXZDXK-070C) and the Tianjin Research Innovation Project for Postgraduate Students (No. 2021YJSS157).

Disclosure

The authors report no conflicts of interest in this work.

References

1. Walkey CD, Chan WC. Understanding and controlling the interaction of nanomaterials with proteins in a physiological environment. *Chem Soc Rev*. 2012;41(7):2780–2799. doi:10.1039/C1CS15233E
2. Liu Q, Zhu H, Qin J, Dong H, Du J. Theranostic vesicles based on bovine serum albumin and poly(ethylene glycol)-block-poly(L-lactic-co-glycolic acid) for magnetic resonance imaging and anticancer drug delivery. *Biomacromolecules*. 2014;15(5):1586–1592. doi:10.1021/bm500438x
3. Pasquini L, Napolitano A, Visconti E, et al. Gadolinium-based contrast agent-related toxicities. *CNS Drugs*. 2018;32(3):229–240. doi:10.1007/s40263-018-0500-1
4. Davies J, Siebenhandl-Wolff P, Tranquart F, Jones P, Evans P. Gadolinium: pharmacokinetics and toxicity in humans and laboratory animals following contrast agent administration. *Arch Toxicol*. 2022;96(2):403–429. doi:10.1007/s00204-021-03189-8
5. Zou Z, Ma L. Nephrogenic systemic fibrosis: review of 408 biopsy-confirmed cases. *Indian J Dermatol*. 2011;56(1):65–73. doi:10.4103/0019-5154.77556
6. Grobner T. Gadolinium—a specific trigger for the development of nephrogenic fibrosing dermopathy and nephrogenic systemic fibrosis? *Nephrol Dial Transplant*. 2006;21(4):1104–1108. doi:10.1093/ndt/gfk062
7. Gulani V, Calamante F, Shellock FG, Kanal E, Reeder SB; International Society for Magnetic Resonance in M. Gadolinium deposition in the brain: summary of evidence and recommendations. *Lancet Neurol*. 2017;16(7):564–570. doi:10.1016/S1474-4422(17)30158-8
8. Mendichovszky IA, Marks SD, Simcock CM, Olsen OE. Gadolinium and nephrogenic systemic fibrosis: time to tighten practice. *Pediatr Radiol*. 2008;38(5):489–496; quiz 602–483. doi:10.1007/s00247-007-0633-8
9. Runge VM. Critical questions regarding gadolinium deposition in the brain and body after injections of the gadolinium-based contrast agents, safety, and clinical recommendations in consideration of the EMA's pharmacovigilance and risk assessment committee recommendation for suspension of the marketing authorizations for 4 linear agents. *Invest Radiol*. 2017;52(6):317–323. doi:10.1097/RLI.0000000000000374
10. Shao YZ, Liu LZ, Song SQ, et al. A novel one-step synthesis of Gd³⁺-incorporated mesoporous SiO₂ nanoparticles for use as an efficient MRI contrast agent. *Contrast Media Mol Imaging*. 2011;6(2):110–118. doi:10.1002/cmim.412
11. Liu S, Yue H, Ho SL, et al. Enhanced tumor imaging using glucosamine-conjugated polyacrylic acid-coated ultrasmall gadolinium oxide nanoparticles in magnetic resonance imaging. *Int J Mol Sci*. 2022;23(3):1792.
12. Otsubo K, Kishimoto J, Ando M, et al. Nintedanib plus chemotherapy for nonsmall cell lung cancer with idiopathic pulmonary fibrosis: a randomised Phase 3 trial. *Eur Respir J*. 2022;60(6). doi:10.1183/13993003.00380-2022
13. Gianni L, Mansutti M, Anton A, et al. Comparing neoadjuvant nab-paclitaxel vs paclitaxel both followed by anthracycline regimens in women with ERBB2/HER2-negative breast cancer—the Evaluating Treatment With Neoadjuvant Abraxane (ETNA) trial: a randomized phase 3 clinical trial. *JAMA Oncol*. 2018;4(3):302–308. doi:10.1001/jamaoncol.2017.4612
14. Ghaghada KB, Ravoori M, Sabapathy D, Bankson J, Kundra V, Annapragada A. New dual mode gadolinium nanoparticle contrast agent for magnetic resonance imaging. *PLoS One*. 2009;4(10):e7628. doi:10.1371/journal.pone.0007628
15. Yousuf I, Bashir M, Arjmand F, Tabassum S. Multispectroscopic insight, morphological analysis and molecular docking studies of Cu-II-based chemotherapeutic drug entity with human serum albumin (HSA) and bovine serum albumin (BSA). *J Biomol Struct Dyn*. 2019;37(12):3290–3304. doi:10.1080/07391102.2018.1512899
16. Azevedo C, Nilsen J, Grevys A, Nunes R, Andersen JT, Sarmiento B. Engineered albumin-functionalized nanoparticles for improved FcRn binding enhance oral delivery of insulin. *J Control Release*. 2020;327:161–173. doi:10.1016/j.jconrel.2020.08.005

17. Sun ZC, Zheng WS, Zhu GS, et al. Albumin broadens the antibacterial capabilities of nonantibiotic small molecule-capped gold nanoparticles. *Acs Appl Mater Inter*. 2019;11(49):45381–45389. doi:10.1021/acsami.9b15107
18. Paul M, Itoo AM, Ghosh B, Biswas S. Current trends in the use of human serum albumin for drug delivery in cancer. *Expert Opin Drug Deliv*. 2022;19(11):1449–1470. doi:10.1080/17425247.2022.2134341
19. Wei HQ, Zhang B, Lei M, et al. Visible-light-mediated nano-biomineralization of customizable tough hydrogels for biomimetic tissue engineering. *Acs Nano*. 2022;16(3):4734–4745. doi:10.1021/acsnano.1c11589
20. Abou Neel EA, Aljabo A, Strange A, et al. Demineralization-rem mineralization dynamics in teeth and bone. *Int J Nanomed*. 2016;11:4743–4763. doi:10.2147/IJN.S107624
21. Chu CC, Su M, Zhu J, et al. Metal-organic framework nanoparticle-based biomineralization: a new strategy toward cancer treatment. *Theranostics*. 2019;9(11):3134–3149. doi:10.7150/thno.33539
22. Zhang BB, Jin HT, Li Y, Chen BD, Liu SY, Shi DL. Bioinspired synthesis of gadolinium-based hybrid nanoparticles as MRI blood pool contrast agents with high relaxivity. *J Mater Chem*. 2012;22(29):14494–14501. doi:10.1039/c2jm30629h
23. Zhang H, Wang T, Zheng Y, Yan C, Gu W, Ye L. Comparative toxicity and contrast enhancing assessments of Gd(2)O(3)@BSA and MnO(2)@BSA nanoparticles for MR imaging of brain glioma. *Biochem Biophys Res Commun*. 2018;499(3):488–492. doi:10.1016/j.bbrc.2018.03.175
24. Chen L, Zhou XJ, Nie W, et al. Marriage of albumin-gadolinium complexes and MoS₂ nanoflakes as cancer theranostics for dual-modality magnetic resonance/photoacoustic imaging and photothermal therapy. *Acs Appl Mater Inter*. 2017;9(21):17786–17798. doi:10.1021/acsami.7b04488
25. Ma N, Liu J, He W, et al. Folic acid-grafted bovine serum albumin decorated graphene oxide: an efficient drug carrier for targeted cancer therapy. *J Colloid Interface Sci*. 2017;490:598–607. doi:10.1016/j.jcis.2016.11.097
26. Wang J, Zhang BB. Bovine serum albumin as a versatile platform for cancer imaging and therapy. *Curr Med Chem*. 2018;25(25):2938–2953. doi:10.2174/0929867324666170314143335
27. Liu LS, Bi YK, Zhou MR, et al. Biomimetic human serum albumin nanoparticle for efficiently targeting therapy to metastatic breast cancers. *Acs Appl Mater Inter*. 2017;9(8):7424–7435. doi:10.1021/acsami.6b14390
28. Hou Z, Zhou M, Ma Y, et al. Size-changeable nanoprobe for the combined radiotherapy and photodynamic therapy of tumor. *Eur J Nucl Med Mol Imaging*. 2022;49(8):2655–2667. doi:10.1007/s00259-022-05830-9
29. Wen Y, Dong H, Li Y, Shen A, Li Y. Nano-assembly of bovine serum albumin driven by rare-earth-ion (Gd) biomineralization for highly efficient photodynamic therapy and tumor imaging. *J Mater Chem B*. 2016;4(4):743–751. doi:10.1039/C5TB01962A
30. Li M, Liu Z, Wu Y, et al. In vivo imaging of astrocytes in the whole brain with engineered AAVs and diffusion-weighted magnetic resonance imaging. *Mol Psychiatr*. 2022. doi:10.1038/s41380-022-01580-0
31. Boucher M, Geffroy F, Preveral S, et al. Genetically tailored magnetosomes used as MRI probe for molecular imaging of brain tumor. *Biomaterials*. 2017;121:167–178. doi:10.1016/j.biomaterials.2016.12.013
32. Brown PL, Kiyatkin EA. Brain temperature change and movement activation induced by intravenous cocaine delivered at various injection speeds in rats. *Psychopharmacology*. 2005;181(2):299–308. doi:10.1007/s00213-005-2244-0
33. Zhou L, Yang T, Wang J, et al. Size-tunable Gd(2)O(3)@Albumin nanoparticles conjugating chlorin e6 for magnetic resonance imaging-guided photo-induced therapy. *Theranostics*. 2017;7(3):764–774. doi:10.7150/thno.15757
34. Pan J, Wang J, Fang K, et al. RNA m(6)A alterations induced by biomineralization nanoparticles: a proof-of-concept study of epitranscriptomics for nanotoxicity evaluation. *Nanoscale Res Lett*. 2022;17(1):23. doi:10.1186/s11671-022-03663-x
35. Sun SK, Dong LX, Cao Y, Sun HR, Yan XP. Fabrication of multifunctional Gd₂O₃/Au hybrid nanoprobe via a one-step approach for near-infrared fluorescence and magnetic resonance multimodal imaging in vivo. *Anal Chem*. 2013;85(17):8436–8441. doi:10.1021/ac401879y
36. Wang Y, Yang CX, Yan XP. Hydrothermal and biomineralization synthesis of a dual-modal nanoprobe for targeted near-infrared persistent luminescence and magnetic resonance imaging. *Nanoscale*. 2017;9(26):9049–9055. doi:10.1039/C7NR02038D
37. Liu M, Zhao ZQ, Fang W, Liu S. Novel approach for (99m)Tc-labeling of red blood cells: evaluation of (99m)Tc-4SABoroxime as a blood pool imaging agent. *Bioconjug Chem*. 2017;28(12):2998–3006. doi:10.1021/acs.bioconjugchem.7b00601
38. Rahmer J, Antonelli A, Sfara C, et al. Nanoparticle encapsulation in red blood cells enables blood-pool magnetic particle imaging hours after injection. *Phys Med Biol*. 2013;58(12):3965–3977. doi:10.1088/0031-9155/58/12/3965
39. Aryal S, Stigliano C, Key J, et al. Paramagnetic Gd(3+) labeled red blood cells for magnetic resonance angiography. *Biomaterials*. 2016;98:163–170. doi:10.1016/j.biomaterials.2016.05.002
40. Jayaprakash V, Costalonga M, Dhulipala S, Varanasi KK. Enhancing the injectability of high concentration drug formulations using core annular flows. *Adv Healthc Mater*. 2020;9(18):e2001022. doi:10.1002/adhm.202001022
41. Sun Y, Feng W, Yang P, Huang C, Li F. The biosafety of lanthanide upconversion nanomaterials. *Chem Soc Rev*. 2015;44(6):1509–1525. doi:10.1039/C4CS00175C
42. Lu C, Xu X, Zhang T, Wang Z, Chai Y. Facile synthesis of superparamagnetic nickel-doped iron oxide nanoparticles as high-performance T(1) contrast agents for magnetic resonance imaging. *J Mater Chem B*. 2022;10(10):1623–1633. doi:10.1039/D1TB02572D

International Journal of Nanomedicine

Dovepress

Publish your work in this journal

The International Journal of Nanomedicine is an international, peer-reviewed journal focusing on the application of nanotechnology in diagnostics, therapeutics, and drug delivery systems throughout the biomedical field. This journal is indexed on PubMed Central, MedLine, CAS, SciSearch®, Current Contents®/Clinical Medicine, Journal Citation Reports/Science Edition, EMBASE, Scopus and the Elsevier Bibliographic databases. The manuscript management system is completely online and includes a very quick and fair peer-review system, which is all easy to use. Visit <http://www.dovepress.com/testimonials.php> to read real quotes from published authors.

Submit your manuscript here: <https://www.dovepress.com/international-journal-of-nanomedicine-journal>